An Adaptive Impedance Matching System for Vehicular Power Line Communication

Nima TaheriNejad, *Member, IEEE,* Lutz Lampe, *Senior Member, IEEE,* and Shahriar Mirabbasi, *Member, IEEE*

***Abstract*—Vehicular Power Line Communication (VPLC) is being considered as a potential solution to mitigate the increase of complexity and cost of the automotive wiring harness caused by the growth of the number of electronic devices and sensors deployed inside vehicles. This is because VPLC reuses power cables for data communication and thus avoids the need for additional communication wires. This reuse does not come without problems though. One of the challenges for VPLC is the time, frequency and location dependency of the access impedance, which can cause severe impedance mismatch for the communication signal. Impedance mismatch degrades the signal-to-noise-power ratio at the communication receiver and thus affects transmission reliability. Due to the variable nature of the access impedance, a fixed matching circuit will be inefficient. Hence, in this work we present an *adaptive* impedance matching system which improves the communication-signal transfer from the transmitting to the receiving device. The system is evaluated via simulations for a wide range of access impedance test points and S-parameters of VPLC networks obtained in previous measurement campaigns. Our simulation results demonstrate that the presented adaptive matching system is able to achieve VPLC signal-power transfer within 30% of the theoretical optimum. This translates to a power gain, up to a factor of 10, which is larger than that of other solutions reported in the literature.**

***Index Terms*—Vehicular power line communication, access impedance, impedance mistmatch, adaptive impedance matching.**

I. Introduction

THE use of power lines for communication purposes is a concept dating back to the early 1900s [3]. It has widely been applied for power-grid monitoring and control; including smart meter reading, home and industry automation, and in-home multimedia communication [4], [5]. The significant growth of the number of electronic devices and sensors in vehicles [6]–[8], which is further spurred by the increasing role of electric vehicles in the automotive market, has stimulated interest, research, and development activities in the field of Vehicular Power Line Communication (VPLC) [9]–[20]. Since VPLC reuses power cables and thus avoids the need for installing additional wires dedicated for data communication, it is considered as a means to reduce cost and complexity of the vehicle wiring harness. On the negative side, VPLC is affected by transmission channel imperfections, which includes impulsive noise [17], [21], frequency selectivity of the channel transfer function [14], [16], [18]–[20], and time and location dependent network access impedance [22], [23]. The latter causes a general impedance mismatch for VPLC transmitters and receivers, which results in sub-optimal signal coupling from the transmitter to the network and from the network to the receiver, which in turn weakens the PLC signal transfer. While channel frequency-selectivity and noise can be addressed through the design of appropriate transmission formats and signal processing, impedance mismatch requires the use of impedance matching circuits at VPLC transmitters and receivers. However, conventional matching circuits using fixed passive elements are not effective due to the variability of the access impedance with time and location, caused by time-varying network loads and signal reflections in the power line.

In this paper, we present and evaluate an adaptive impedance matching design that can adjust the matching circuits for each instance of access impedance as monitored by its sensing unit. Preliminary results of our design were presented in [1], [2]. We consider both matching at the transmitter side for signal coupling and at the receiver side for signal decoupling, and discuss the simultaneous operation of transmitter and receiver-side impedance matching. To demonstrate the merit of our design, we use the data obtained in our measurement campaigns [18], [23] and test the system for a wide range of access impedance values. The bandwidth of the matching circuit is also simulated and other important issues such as adaptation delay are discussed.

To put our impedance matching design into context, we continue the discussion with a brief classification of matching approaches and a literature review in the next section. Then, we present our approach to the matching problem in Section III. Section IV describes the design process and the details of each unit in the system. Extensive simulation results are presented and discussed in Section V. Finally, the paper is concluded by Section VI.

II. Classification of Impedance Matching and Literature Review

The design of coupling circuitry has been studied since the first uses of power line communications [4, Ch. 4]. Since VPLC operates over DC power systems, theoretically a single capacitor could be used to couple and decouple the high-frequency communication signal. However, this would be sub-optimal considering the communication signal transfer. To

This work was supported in part by the AUTO21 Network of Centres of Excellence, the Natural Sciences and Engineering Research Council of Canada (NSERC) and the Partners for the Advancement of Collaborative Engineering Education (PACE) program. CAD tool support and access to technology was facilitated by CMC Microsystems.

The authors are/were with the Department of Electrical and Computer Engineering at the University of British Columbia. N. TaheriNejad is now with the Vienna University of Technology. Email: nima.taherinejad@tuwien.ac.at, {lampe,shahriar}@ece.ubc.ca

Parts of this work have been published at the IEEE International Symposium of Power Line Communicaion (ISPLC) in 2012 [1] and 2014 [2].

This article has been accepted for publication in a future issue of this journal, but has not been fully edited. Content may change prior to final publication. Citation information: DOI 10.1109/TVT.2016.2562629, IEEE Transactions on Vehicular Technology

TABLE I
CLASSIFICATION OF IMPEDANCE MATCHING SOLUTIONS.

Criterion	Classes	Brief Description
Method	Numerical	Real Frequency Technique
	Analytical	Circuit models
Load/Source Impedance Type	Double	Complex/Complex
	Single	Complex/Resistive
	Insertion Loss	Resistive/Resistive
Structure	Fixed	One circuit topology
	Flexible	Changing topologies
Implementation	Passive	On-chip, off-chip (bulky)
	Active	Easily integrated
Bandwidth	Narrowband	
	Wideband	

TABLE II
COMPARING CURRENT WORK TO OTHER RELATED WORKS.

Work	[29]	[22]	[30]	[31]
Methodology	Analytical	Analytical	Numerical	Analytical
Impedance Type	Insertion Loss	Single	Single	Single
Structure	Fixed	Fixed	Flexible	Flexible
Implementation	Passive	Combination	Passive	Combination
Bandwidth	Narrow	Narrow	Wide	Narrow
Notes	Bulky, heavy and expensive transformers	Transformers used, alleviated method	Complex control system (M-PSO)	Control system not discussed

address this issue, a coupling circuit is necessary that is able to match the impedance between the network and the VPLC modems. In this section, we first briefly introduce the general concept of impedance matching, and then review some of the PLC matching systems presented in the literature.

A. Impedance Matching - Concept and Classification

Considering a power source with an internal impedance connected to a load and writing the respective circuit solution, it can be easily derived that maximum power is transferred to the load if the load impedance is equal to complex conjugate of the source internal impedance. In the context of VPLC, at the transmitter, the load is the vehicle harness. Its Thévenin/Norton equivalent impedance, i.e., the access impedance, is considered as the load impedance, and this should be complex-conjugate matched to the transmitter's internal impedance. At the receiver side, the load is the receiver's input impedance, which should be complex-conjugate matched to the harness access impedance as seen from the receiver side. Using fixed VPLC transmitter and receiver impedances, e.g., $50\ \Omega$, will most often result in impedance mismatch, since the access impedance is dependent on the point of coupling/decoupling and varies with time. Therefore, to maximize signal-power transmission into the network at the transmitter side and out of the network at the receiver side adaptive impedance matching circuits are needed. In order to match the impedance without any power loss, lossless passive elements need to be used, cf. e.g. [24], [25, Ch. 5], [26], [27].

Table I shows a classification of impedance matching solutions, according to the criterion shown in the first column. Numerical methods use mathematics (non-linear optimization simulator in case of Real Frequency Technique [28] example) for finding an optimum matching solution over a given range of frequency, whereas to this end, analytical methods use circuit models for the channel and devices in the design. In terms of source and load impedance, the matching could be done for impedances of resistive to resistive (Insertion Loss), resistive to complex (Single Matching) or complex to complex (Double Matching) nature. The structure (topology of the circuit) could be fixed or flexible, where in the latter case, the circuit topology changes based on the needs. Matching circuits can be implemented using passive elements (RLC) or active elements (such as active inductors and opamps), and the objective could be matching over a relatively narrow or wide bandwidth. We refer the reader to [1] for more details on each class. All the classes could potentially be used in an appropriate setup to address a matching problem. The rest of this section is dedicated to a review of adaptive impedance matching systems, specifically those which were designed for PLC applications. Table II presents a summary of these works and how they fit into classes from Table I. The distinguishing features of these works are briefly reviewed in Section II-B, and we invite the reader to consult [1] for a longer review or the given reference of each work for full details.

B. Related Works

In earlier approaches such as the one by Mavretic et al. [29], PLC systems were designed mostly with a focus on resistive loads and sources (insertion loss problem). Use of bulky, heavy and expensive transformers was also a common practice. To address this issue, Park et al. [22] use a Voltage-Controlled General Impedance Converter (VCGIC), as proposed in [32], to build active inductors in a more compact way as opposed to passive inductors. One of the limiting factors for active inductors however, is the maximum current and voltage supported by operational amplifiers used in the circuit. They try to solve this problem with the addition of a fixed passive inductor and a transformer, which would be smaller considering the simultaneous use of the active inductor. However, by using a transformer and an off-chip inductor they forfeit part of the advantages gained from applying an active inductor.

Some efforts were also turned toward wide-band impedance matching systems. For example, Araneo et al. [30] use an LC-ladder structure and a numerical method to fit the structure parameters. Numerical optimization is accomplished with a meta-particle swarm optimization (M-PSO) algorithm. As illustrated in Fig. 1 (results taken from [30]), this method can achieve an improved power transmission over a relatively wide frequency range. However, using a numerical method requires a digital processor capable of solving the optimization problems fast enough to provide the solution within a reasonable delay time. Aiming at inexpensive, small area integrated solutions this can be considered as a disadvantage.

Finally, our approach for narrowband matching, first proposed in [1], was adopted by Nisbet et al. in [31]. The capability of transformerless impedance matching (at the transmitter side) is demonstrated for a range of access impedances. However, it is not entirely clear in what way the design

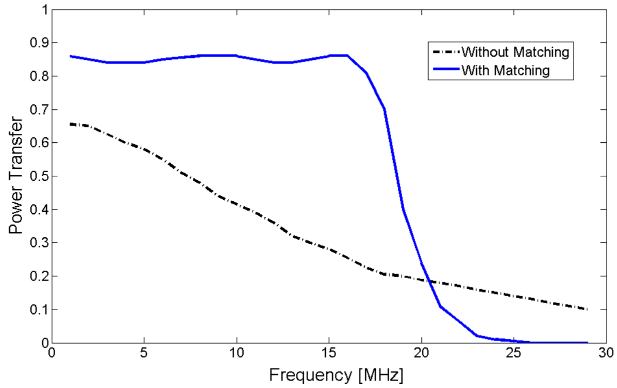

Fig. 1. Power transfer between modem and power line with (blue solid line) and without (black dashed line) Araneo's wideband impedance matching. Results taken from [30, Fig. 5].

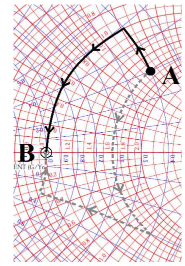

Fig. 2. Matching problem demonstrated in the Smith chart. From a given impedance, point A, to the desired impedance, point B, there are several paths (two samples shown) which could be implemented through matching circuits.

extends beyond [1], as the control and some other parts of the system, which have a major impact on the performance, are not explained.

In the following, we build on our previous work in [1], [2], enhance the design for transmitter-side matching and propose a new design for receiver-side matching. We will then elaborate on the details of the control system. Finally, we present simulations for our impedance-matching solutions and demonstrate the suitability of the design even for wideband applications.

III. Our Approach to The Matching Problem

In this section we first introduce our approach to solve the matching problem at one end of the communication system. At the transmitter side, the source and its internal impedance interact with the network, which is represented by its equivalent impedance, i.e., the access impedance. On the receiver side, the network is represented with its Thevenin equivalent circuit and interacts with the receiver's input impedance. Then, we will explain that, based on results from our previous measurement campaigns, matching at one side of the network does not have a significant impact on matching at the other side in VPLC. Hence, independent matching at the transmitter and the receiver will be a practically meaningful solution for the matching problem in VPLC applications.

A. Impedance Matching at One End

There are several ways to approach the matching problem. A useful tool that aids the understanding of the underlying concepts is the Smith chart. The Smith chart efficiently visualizes the location of impedances and the effect of adding various impedances to a network. Therefore, in the following, we will use Smith chart to facilitate the understanding of the derivation of our impedance matching system. We would like to emphasize however, that the Smith chart is not part of the actual impedance matching implementation.

The matching problem is finding a circuit that changes an impedance seen at one of its ports to another impedance at the other port. In the Smith chart this circuit can be represented as a path going from a point A, the original impedance, to the desired point B, the matched impedance. The latter is often at the center of the Smith chart. Figure 2 shows two different sample paths from a point A to a point B. One can find many other paths connecting these two points. However, a lossless solution can be obtained by only traversing constant conductance or constant resistance contours. This consideration reduces the number of possible paths, but there are still many options. Another limiting factor to be considered can be the number of moves along these contours. Since each move represents a series or parallel non-resistive element in the matching circuit, more moves entail the use of more components and consequently result in a more complex circuit structure. This also imposes an extra burden to the control logic for adaptation. Therefore, matching with fewer moves (e.g., two for the black solid line in Fig. 2) is preferred over matching with more moves (e.g., three for the gray dotted line in Fig. 2).

Following the above rationale we adopt a two-move strategy to perform the matching. The first move is along a constant conductance contour to reach the constant resistance contour of the matching target, or along a constance resistance contour to reach the constant conductance contour of the matching target. This compensates for the real part of the impedance mismatch. The second move is along the constant resistance or conductance contour until the matching target is reached, and it thus compensates for the imaginary part of the mismatch. Constant conductance moves are accomplished through a parallel inductor or capacitor, and constant resistance moves are achieved with a series inductor or capacitor.

Normalizing the Smith chart with the target impedance[1], so that it is represented by the center point of the chart, Figure 3 shows the perfect-match conductance and resistance circles in red and purple, respectively. Therefore, our first move from any point is to reach one of these circles. To choose the path to these circles, the location of the original impedance point in the Smith chart is important, since it determines the type of element used for achieving this move. It matters whether the original impedance value is inside or outside of one of the circles and whether it is above or below the green line shown in Figure 3 (for a resistive target impedance, above and below the green line means inductive and capacitive original impedances,

[1] The target impedance is the modem impedance for our application, and it is assumed to be a given design parameter. This information can be obtained from the modem specifications, which includes their input and output equivalent Thévenin/Norton models.

This article has been accepted for publication in a future issue of this journal, but has not been fully edited. Content may change prior to final publication. Citation information: DOI 10.1109/TVT.2016.2562629, IEEE Transactions on Vehicular Technology

TABLE III
COMBINATION OF ELEMENTS IN THE CIRCUIT TO ACHIEVE MATCHING IF NETWORK ACCESS IMPEDANCE IS IN DIFFERENT REGIONS SHOWN IN FIGURE 2.

	Transmitter-side matching	**Receiver-side matching**
Region	Combination	Combination
1	series inductor followed by a parallel capacitor	parallel inductor followed by series capacitor
2	series capacitor followed by a parallel capacitor	parallel inductor followed by a series inductor
3	parallel capacitor followed by a series capacitor	series inductor followed by a parallel inductor
4	parallel inductor followed by a series capacitor	series inductor followed by a parallel capacitor
5	parallel capacitor followed by a series inductor	series capacitor followed by a parallel inductor
6	parallel inductor followed by a series inductor	series capacitor followed by a parallel capacitor
7	series inductor followed by a parallel inductor	parallel capacitor followed by a series capacitor
8	series capacitor followed by a parallel inductor	parallel capacitor followed by a series inductor

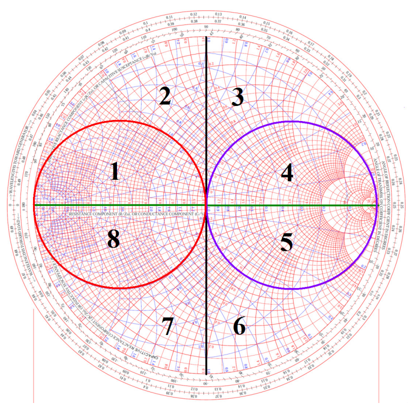

Fig. 3. Smith chart divided into 8 regions, to categorize different movements.

respectively). Furthermore, for the regions outside the circles, the moves are determined by which of the two circles is closer. Hence, the Smith chart is divided into the 8 regions shown in Figure 3.

For transmitter-side impedance matching, we move from the network access impedance (the original impedance) tothe internal impedance of the modem (i.e., the target impedance, which is obtained from the modem specification). Depending on the region of the Smith chart into which the access impedance falls, we apply the combination of elements in the matching circuit shown in top part of Table III. These combinations will bring us to the centre of the Smith chart. To reuse the same circuitry for receiver-side matching, the original and the target impedance change their roles and we need to move from the centre of the Smith chart (corresponding to the known impedance of the receiving modem, which is again a given parameter in the modem specification) to the access impedance point in the Smith chart. This is accomplished by traversing the paths from transmitter-side matching in reverse direction, for which the circuit-element combinations are shown in the right-most part of Table III. We will apply the insights gained from the Smith chart analysis when designing the impedance matching and control units in Section IV.

B. Impedance Matching at Both Ends

The VPLC network access impedance is clearly dependent on the loads connected to the power harness, which makes it dependent on the state of these loads and thus time varying. Measurement results in e.g. [16, Figs. 8] and [23, Figs. 5 and 6] show such dependencies as a function of the vehicle ignition state. This means that strictly speaking transmitter and receiver-side matching should be performed jointly. However, it is interesting to look at the effect of changing the load impedance at one end (via impedance matching) onto the access impedance at the other end of the communication link.

To this end, we consider S-parameter channel data obtained in our measurement campaigns reported in [18], [23]. In particular, we compute the reflection coefficients [25]

$$\Gamma_{\text{in}} = S_{11} + \frac{S_{12}S_{21}}{1 - S_{22}\Gamma_{\text{L}}}\Gamma_{\text{L}} \tag{1}$$

at the transmitter side of the network, as a function of the reflection coefficient of the load impedance Γ_{L}, and

$$\Gamma_{\text{out}} = S_{22} + \frac{S_{12}S_{21}}{1 - S_{22}\Gamma_{\text{S}}}\Gamma_{\text{S}} \tag{2}$$

at the receiver side of the network, as a function of the source reflection coefficient Γ_{S}. S_{ij} are the measured S-parameters and the relationship between a reflection coefficient Γ and an impedance Z is

$$\Gamma = (Z - Z_0)/(Z + Z_0)\ , \tag{3}$$

where the reference impedance $Z_0 = 50\ \Omega$ for our measurements [18], [23]. For the following, we choose Γ_{L} and Γ_{S} corresponding to the six impedance values $\{0.1, 1, 10, 50, 100, 250\}\ \Omega$, which cover the whole range for the real part of access impedances that we have seen in our measurement campaigns. In addition, we consider the case of perfect impedance matching, for which [33]

$$\Gamma_{\text{S}} = \frac{B \pm \sqrt{B^2 - 4|C|^2}}{2C}\ , \tag{4}$$

where

$$\begin{array}{rcl} B &=& 1 + |S_{11}|^2 - |S_{22}|^2 - |S_{11}S_{22} - S_{21}S_{12}|^2 \\ C &=& S_{11} - S_{22}^{*}|S_{11}S_{22} - S_{21}S_{12}| \end{array}\ , \tag{5}$$

and Γ_{L} has the same form as (4) with S_{11} and S_{22} swapped in (5).

The effect of varying the termination impedance at one side of the VPLC link according to the seven cases specified above is shown in Table IV. We consider four links of a hybrid-electric vehicle measured in [18] and four links of a combustion-engine vehicle measured in [23], respectively, and the results are the average and maximal deviations for the seven scenarios over the frequency range from 100 kHz to 100 MHz. We observe that the effect of changing the load at one end of the link onto the other end is overall fairly moderate. Even the maximal change is only in one case more

This article has been accepted for publication in a future issue of this journal, but has not been fully edited. Content may change prior to final publication. Citation information: DOI 10.1109/TVT.2016.2562629, IEEE Transactions on Vehicular Technology

TABLE IV
EFFECT OF TERMINATION AT ONE END OF A VPLC LINK ON THE OTHER END FOR SEVERAL MEASURED LINKS. AVERAGE (AVG) AND MAXIMUM (MAX) CHANGE FOR SEVEN TERMINATION IMPEDANCES.

Link (from [18], [23])	Effect on Γ_{in} (%)		Effect on Γ_{out} (%)	
	Avg	Max	Avg	Max
VCU-DMOC	0.08	1.41	0.09	2.11
VCU-DC/DC	0.005	0.67	0.002	0.13
DC/DC-DMOC	0.01	0.11	0.03	0.71
HVBat-DMOC	0.42	6.61	0.19	4.58
Average/Max for [18]	*0.13*	*6.61*	*0.08*	*4.58*
Bat-Cigar	0.05	1.25	0.11	1.13
Bat-Trunk	0.08	3.44	0.18	12.44
Bat-Tail-R	0.02	0.61	0.05	3.56
Bat-Front-L	0.07	1.80	0.20	3.74
Average/Max for [23]	*0.06*	*3.44*	*0.14*	*12.44*
Total Average/Max	**0.10**	**6.61**	**0.11**	**12.44**

than 10%, which is due to deep notches seen in the channel transfer function. These results suggest that performing impedance matching independently at the transmitter and the receiver side should not incur notable performance penalties compared to joint matching at both ends of the link. Since the latter would require the exchange of access impedance measurements, we prefer and pursue the independent matching approach in the following.

IV. SYSTEM DESIGN

Having established the basic principles of our approach to impedance matching, in this section we explain the details of our matching system.

A. Basic Structure and Operation

The block diagram of the proposed adaptive impedance matching system is shown in Figure 4. It is implemented at the transmitter and receiver side and each system consists of three main units: measurement unit, impedance matching unit and control unit. To enable the matching, we assume that the communication device sends a tone at a frequency of f_c, which is the centre frequency for the band in which matching is to be achieved. When the measurement unit is settled, the control unit adjusts the matching circuit elements in the matching unit. The adjustment at a considered device can be different depending on whether transmitter-side or receiver-side matching is performed. Hence, a device could have two different matching units, one for transmission and one for reception, or the same matching unit can be used but its setting would change from transmission to reception. After setting the values in the matching unit, devices go to their normal state of transmission or reception of data. Adaptation of the matching circuit can be done periodically, or on demand when transmitting or receiving data.

B. Measurement Unit

The measurement unit senses physical parameters and provides this information to the control unit for decision making. Figure 5 shows the structure of the measurement unit, which can be divided into the sensing unit and the interpretation unit.

The details of the sensing unit are shown in Figure 6. A very small resistor (e.g. 0.1 to 1 Ω) is used for sensing, and two

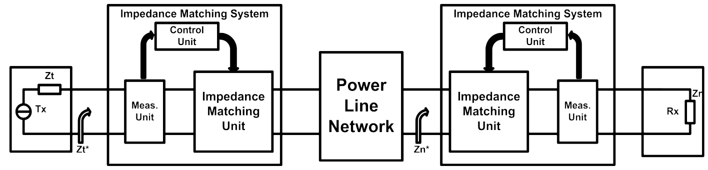

Fig. 4. Block diagram of the proposed adaptive impedance matching system for the transmitter and receiver side. $Z_{\rm t}$ and $Z_{\rm n}$ denote the source impedance at the transmitter and network access impedance seen from the receiver, respectively. $Z_{\rm t}^*$ and $Z_{\rm n}^*$ indicate the *desired* impedance matching at the transmitter and receiver, respectively.

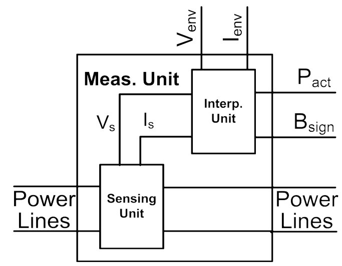

Fig. 5. Block diagram of the measurement unit.

operational amplifiers (Op-Amps) amplify the sensed signals. One Op-Amp measures the voltage across the resistor, from which the current going through it, $I_{\rm s}$ is obtained. The other Op-Amp measures the voltage between the input node and the reference node (ground), $V_{\rm s}$. Given the single-tone signal, we have

$$V_{\rm s}(t) = \sqrt{2}V_{\rm env}\cos(2\pi f_{\rm c}t+\phi) \quad (6)$$
$$I_{\rm s}(t) = \sqrt{2}I_{\rm env}\cos(2\pi f_{\rm c}t)\ . \quad (7)$$

The interpretation unit is supplied with the voltage and current signals generated by the sensing unit and outputs four control signals, $V_{\rm env}$, $I_{\rm env}$, $P_{\rm act}$ and $B_{\rm sign}$, that are used by the control unit (see Fig. 4). $V_{\rm env}$ and $I_{\rm env}$ are the envelop values of the measured voltage and current signals in (6) and (7), and generated by the circuit shown in Figure 7. Multiplying $V_{\rm s}$ and $I_{\rm s}$ gives the instantaneous source power

$$\begin{aligned} P_{\rm s}(t) &= 2KV_{\rm env}I_{\rm env}\cos(2\pi f_{\rm c}t+\phi)\cos(2\pi f_{\rm c}t) \\ &= KV_{\rm env}I_{\rm env}\left[\cos(2\pi(2f_{\rm c})t+\phi)+\cos(\phi)\right]\ , \quad (8)\end{aligned}$$

where K is a constant denoting the overall gain of the multiplier circuit. This is followed by low-pass filtering, which provides the active-power measurement ("$*$" denotes convolution)

$$P_{\rm act}(t) = (h_{\rm LP} * P_{\rm s})(t)\ , \quad (9)$$

which converges to $KV_{\rm env}I_{\rm env}\cos(\phi)$. The circuit-level block diagram for the active-power measurement is shown in Figure 8. Finally, $B_{\rm sign}$ is a Boolean variable that indicates whether a load is inductive ($B_{\rm sign} = 0$) or capacitive ($B_{\rm sign} = 1$). The circuit shown in Figure 9 generates $B_{\rm sign}$ by comparing the values of voltage and current at the zero crossings.

This article has been accepted for publication in a future issue of this journal, but has not been fully edited. Content may change prior to final publication. Citation information: DOI 10.1109/TVT.2016.2562629, IEEE Transactions on Vehicular Technology

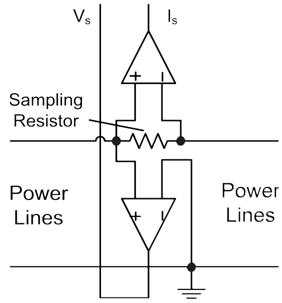

Fig. 6. Circuit-level block diagram of the sensing unit.

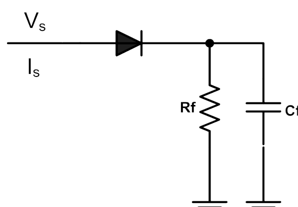

Fig. 7. Envelop detecting circuit used in the interpretation unit. In this paper the values were selected as $R_{\mathrm{f}} = 1$ kΩ and $C_{\mathrm{f}} = 1.4$ pF.

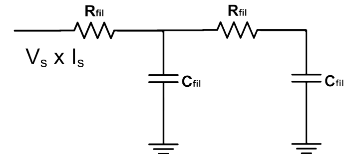

Fig. 8. Second order low-pass RC filter for active power measurement P_{act}. Used values were selected as $R_{\mathrm{fil}} = 10$ kΩ and $C_{\mathrm{fil}} = 6$ pF.

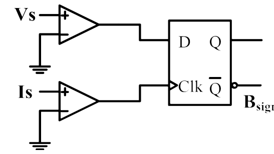

Fig. 9. The circuit used to discern capacitive versus inductive loads based on zero crossings. The output is "1" if the load is capacitive and "0" if inductive.

C. Matching Unit

As explained in Section III-A, an arrangement of L-structured inductors and/or capacitors can perform the impedance matching leading to the maximum active power transfer between modem and the network. Figure 10 shows the corresponding circuit structure that can be used for this impedance matching. This unit turns the bias voltages B_{L}, B_{R} and B_{M} into the actual capacitance and inductance values according to

$$\mathrm{LP} = \frac{Z_0}{2\pi f_{\mathrm{c}} V_{\mathrm{B}}}, \tag{10}$$

$$\mathrm{CP} = \frac{V_{\mathrm{B}}}{2\pi f_{\mathrm{c}} Z_0}, \tag{11}$$

$$\mathrm{LS} = \frac{V_{\mathrm{B}} Z_0}{2\pi f_{\mathrm{c}}}, \tag{12}$$

$$\mathrm{CS} = \frac{V_{\mathrm{B}} Z_0}{2\pi f_{\mathrm{c}}}, \tag{13}$$

where V_{B} is to be substituted by B_{L}, B_{R} and B_{M} according to Figure 10 and $Z_0 = 50\ \Omega$. The bias voltages and switches shown in Figure 10 are adjusted by the control unit described next.

D. Control Unit

The control unit (see Figure 4) uses the input from the measurement unit to provide the matching unit with control signals that determine the state of the switches as well as the normalized values of the components in the matching circuit shown in Figure 10. This is done by determining the access impedance's value and comparing it to the target impedance. On the Smith chart, this would correspond to the position of the access impedance with respect to the eight different regions in Figure 3.

To this end, first the measured impedances are identified as inductive or capacitive (above or below the green line in Figure 3) using the B_{sign} signal provided by the measurement unit. Next, we determine whether $V_{\mathrm{env}}/I_{\mathrm{env}}$ is smaller or larger than the modem impedance. (In the Smith chart representation this would be whether the impedance is in the left or right-hand side half of the Smith chart, i.e., left or right of the black line in Figure 3.) Writing real and imaginary part of the reflection coefficient $\Gamma = a + \mathrm{j}b$, we have

$$\begin{aligned} Z &= Z_0 \frac{1+\Gamma}{1-\Gamma} = Z_0 \frac{1+a+\mathrm{j}b}{1-a-\mathrm{j}b} \\ \Rightarrow \quad |Z| = \frac{V_{\mathrm{env}}}{I_{\mathrm{env}}} &= |Z_0| \frac{(1+a)^2+b^2}{(1-a)^2+b^2} \\ \Rightarrow \quad \frac{V_{\mathrm{env}}}{I_{\mathrm{env}}} \lesseqgtr |Z_0| &\Leftrightarrow \frac{(1+a)^2+b^2}{(1-a)^2+b^2} \lesseqgtr 1 \\ &\Leftrightarrow a \lesseqgtr 0 \end{aligned} \tag{14}$$

where the reference impedance Z_0 is the impedance of the transmitter/receiver-modem for transmitter/receiver-side matching. Hence, if $V_{\mathrm{env}}/I_{\mathrm{env}}$ is smaller than the modem impedance, then the measured access impedance is located in the left half of Smith chart and vice versa.

Finally, we need to determine whether the real part of impedance or admittance is smaller than the target impedance or admittance or not. On the Smith chart, this corresponds to whether the impedance lies inside or outside the perfect-match circles shown in Figure 3. Starting with the right circle, it can be seen that all the impedances inside have real parts that are larger than that of the modem impedance. Similarly, admittance values inside the left circle have real parts that are bigger than that of the modem admittance. We obtain these real parts from the measured quantities as

$$Z_{\mathrm{r}} = P_{\mathrm{act}}/I_{\mathrm{env}}^2 \tag{15}$$

$$Y_{\mathrm{r}} = P_{\mathrm{act}}/V_{\mathrm{env}}^2 \tag{16}$$

and compare them to the real parts of the modem impedance and admittance, $Z_{\mathrm{r},0}$ and $Y_{\mathrm{r},0}$. That is, we compare the normalized quantities $Z'_{\mathrm{r}} = Z_{\mathrm{r}}/Z_{\mathrm{r},0}$ and $Y'_{\mathrm{r}} = Y_{\mathrm{r}}/Y_{\mathrm{r},0}$ to one.

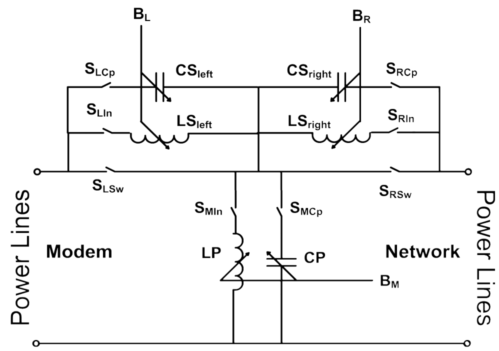

Fig. 10. Circuit structure of the matching unit (see Figure 4).

TABLE V
LOGIC TO DETERMINE LOCATION OF IMPEDANCE IN THE SMITH CHART BASED ON MEASURED VARIABLES.

B_{sign}	$(V_{\text{env}}/I_{\text{env}})/Z_0$	Z'_{r}, Y'_{r}	Region
'1'	≥ 1	$Z'_{\text{r}} \geq 1$	5
		$Z'_{\text{r}} < 1$	6
	< 1	$Y'_{\text{r}} \geq 1$	8
		$Y'_{\text{r}} < 1$	7
'0'	≥ 1	$Z'_{\text{r}} \geq 1$	4
		$Z'_{\text{r}} < 1$	3
	< 1	$Y'_{\text{r}} \geq 1$	1
		$Y'_{\text{r}} < 1$	2

Table V summarizes how we determine the location of the impedance in the Smith Chart. This provides the control unit with all the necessary information regarding the type of moves and their respective order, directions and signs. Together with the matching steps described in Table III, this leads to the logic for the switches in the matching unit in Figure 10 shown in Table VI for the transmitter and the receiver side. The bit stream from most-significant bit (MSB) to the least-significant bit (LSB) shows the status of each switch in the following order: S_{LSw}, S_{LIn}, S_{LCp}, S_{MIn}, S_{MCp}, S_{RIn}, S_{RCp}, S_{RSw}.

The values for the capacitor and inductor elements are also decided by the control unit. To find a relation between inputs, i.e., measured parameters, and assigned values for each element of the matching circuit, the magnitudes of the phase changes (i.e., lengths of moves in the Smith chart) need to be determined. For transmitter-side matching, this means that first the magnitude of the phase change that is necessary to compensate for the real part, in case of mismatch (to arrive at the respective perfect-match circle of resistance or conductance), is estimated. Then, the magnitude of the phase change to move from this new point to the target impedance (traversing on the perfect-match circle to the center, i.e., the perfect match point) is determined. For receiver-side matching, the calculation are the same, but in reverse order, as the matching unit needs to move first from the center towards the target impedance on the perfect-match circle and then to the location of the access impedance.

TABLE VI
LOGIC TABLE FOR SWITCHES IN THE MATCHING UNIT OF THE TRANSMITTER AND THE RECEIVER SIDE. THE BIT STREAM REPRESENTS THE STATUS OF SWITCHES IN FOLLOWING ORDER FROM MSB TO LSB: S_{LSw}, S_{LIn}, S_{LCp}, S_{MIn}, S_{MCp}, S_{RIn}, S_{RCp}, S_{RSw}. "0" REPRESENTS THE OPEN-CIRCUIT STATE OF THE SWITCH, "1" IS THE SHORT-CIRCUIT STATE, AND "X" MEANS THE DON'T CARE STATE.

Region	Switches at Tx	Switches at Rx
1	"1XX01100"	"00110XX1"
2	"1XX01010"	"01010XX1"
3	"01001XX1"	"1XX10100"
4	"00110XX1"	"1XX01100"
5	"01001XX1"	"1XX10010"
6	"01010XX1"	"1XX01010"
7	"1XX10100"	"00101XX1"
8	"1XX10010"	"01001XX1"

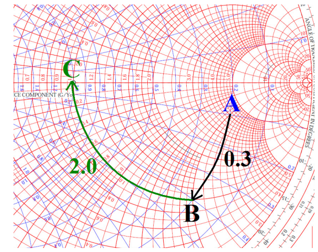

Fig. 11. Illustration of matching an impedance at point A in the Smith chart.

To be specific on how we estimate the lengths of the moves, let us assume that for the transmitter-side, we aim to match an access impedance located at point A in the right-hand side of the Smith chart as shown in Figure 11. The first move needs to change the susceptance from -0.1 at A to -0.4 at point B on the perfect-match circle. We approximate the relation between the susceptance y of the target point B and the normalized conductance $x = Y'_{\text{r}}$ of the access impedance point A by the second order polynomial expression

$$y = 0.01 + 2.15x - 2.15x^2 \; . \tag{17}$$

The magnitude of susceptance change needed for the first move is thus calculated as

$$\Delta_{\text{mov1}} = |Y'_{\text{i}} - y|, \tag{18}$$

where $Y'_{\text{i}} = \sqrt{|Y'|^2 - Y'^2_{\text{r}}}$.

To move from point B to the destination point C, the value of the reactance needs to be changed to zero. The magnitude of this move also can be estimated based on the value of reactance on the perfect match resistance circle, at each conductance circle, i.e. for each $x = Y'_{\text{r}}$. We use the third order polynomial

$$\Delta_{\text{mov2}} = 4.1 - 13.2x + 18.5x^2 - 9.4x^3 \tag{19}$$

to estimate the reactance at each conductance circle and thus the length of the second move.

The previous explanation can be applied to the left half of the Smith chart as well. Impedance and admittance will change place and thus the same polynomials could be used, given that this time $x = Z'_{\text{r}}$ and $\Delta_{\text{mov1}} = |Z'_{\text{i}} - y|$.

The control unit adjusts the values of the bias voltages according to Δ_{mov1} and Δ_{mov2} and passes them to the matching unit, where the capacitance and inductance values are set following Eqs. (10) to (13).

E. Flow Chart Summary

Figure 12 provides the flow chart of the proposed impedance matching solution. It summarizes the details presented in the previous subsections and includes the steps from the time the system measures the access impedance up to the final circuit structure and parameter values which are employed in the final matching circuit.

V. Simulation Results

The proposed impedance matching system was modeled behaviorally, described in Very high speed integrated circuit Hardware Description Language - Analog and Mixed Signal (VHDL-AMS) and simulated in Cadence. In this section, we first describe the access impedance settings we used for our experiments and then present and discuss simulation results. To gain insight into the performance of the matching circuit, three types of simulations results are presented: transmitter-side stand-alone matching, receiver-side stand-alone matching, and concurrent transmitter-side and receiver-side matching.

A. Test Parameters

The shaded area of the Smith chart in Figure 13 shows the range of possible access impedances for the frequency range from 1 MHz to 100 MHz that we have measured for two different vehicles [18], [23]. Since reference impedance is $Z_0 = 50\ \Omega$, the plotted range corresponds to impedances from $\approx 0\ \Omega$ to $250\ \Omega$ for the real part and $-175\ \Omega$ and $+150\ \Omega$ for the imaginary part, respectively. In order to evaluate the performance of the impedance matching under different scenarios, the access impedance points shown in Figure 13 have been selected for simulations[2]. Given the selected impedance values, the matching circuit has been simulated at different frequencies.

Furthermore, in order to evaluate performance of the circuit when operated around the carrier frequency f_c, bandwidth simulations have been performed. For these tests, the impedance matching has been performed at frequency f_c, and then, with matching disabled, the signal frequency was altered around f_c to evaluate the bandwidth performance. Table VII lists the four center frequencies and frequency bands that have been tested in the results presented in Sections V-C and V-D. For each of them, three access impedance values were assumed, according to the maximum, one-tenth of the maximum, and average impedance as measured in [18] for the corresponding frequency f_c. To model the impedances for the entire tested band, we used passive elements (resistors and inductors) with fixed values. The real part of the impedances in Table VII give the resistance values and the inductances are the imaginary part divided by $2\pi f_\mathrm{c}$.

Finally, for simulations of concurrent transmitter-side and receiver-side matching in Section V-E, we use the S-parameters of the links measured in our campaigns [18], [23] to emulate the network characteristics.

[2]We note that we do not have sufficient data to assign probabilities of occurrence to impedance values, and thus it is not clear at this point what cases occur relatively more frequently or less. Hence, we have tried to select impedance values that are spread across a fairly wide range.

TABLE VII
Parameters for bandwidth simulations.

f_c [MHz]	Tested band [MHz]	Access Impedance at f_c [Ω]		
		Maximum	Maximum/10	Average
10	7.5-12.5	$100 + \mathrm{j}60$	$10 + \mathrm{j}6$	$10 + \mathrm{j}20$
30	25-35	$100 + \mathrm{j}45$	$10 + \mathrm{j}4.5$	$20 + \mathrm{j}25$
50	40-60	$260 + \mathrm{j}60$	$26 + \mathrm{j}6$	$40 + \mathrm{j}40$
80	65-95	$150 + \mathrm{j}140$	$15 + \mathrm{j}14$	$75 + \mathrm{j}30$

B. Time-Domain Illustration of Matching

We first illustrate the effect of transmitter-side impedance matching by considering the instantaneous power signal $P_\mathrm{s}(t)$ from (8) at the transmitter side. Figure 14 shows $P_\mathrm{s}(t)$ for an access impedance of 10 Ω and $(75 - \mathrm{j}175)\ \Omega$, respectively. The matching is activated at $t = 150$ ns. We observe that after $t = 150$ ns, the adaptive impedance matching system adjusts the matching circuit such that it improves the power transfer from the source into the network. While for the case of the 10 Ω access impedance (top graph in Figure 14) both the power envelope, i.e., $V_\mathrm{env} I_\mathrm{env}$, and the phase term $\cos(\phi)$ have increased after matching, in the other case (bottom graph in Figure 14), the active power is increased mostly due to better matching of the phase.

Figure 15 illustrates the transmitter-side and receiver-side matching for a communication link by showing the instantaneous and active signal power received by the receiver of the communication link. To model the link, we apply the S-parameters for the VCU-DC/DC link from [18] (see Table IV). As described in Section IV-A, the system uses a preamble signal to perform the matching. In this example, this is done in two stages. First, the transmitter sends the test signal and performs the matching at $t = 1\ \mu$s. As we can see in the left subplot of Figure 15, the power transmitted to the receiver increases due to the larger power inserted into the network from the transmitter side. Then, the test signal is sent from the receiver side at $t = 2\ \mu$s. Accordingly, in the middle subplot of Figure 15 the power received at the receiver is negative as it is injecting power during this period. Note the different y-axis scale for this subplot, which is due to the signal measured before it undergoes channel attenuation. Matching is performed at $t = 3.2\ \mu$s. Finally, the system goes into operation mode where communication could be performed at $t = 4\ \mu$s (right subplot). Overall, the power transfer from the transmitter to the receiver is tripled after both matching circuits have been adapted (after $t = 4\ \mu$s) compared to the original state without matching (before $t = 1\ \mu$s).

We note that the active power shown in Figure 15 is $P_\mathrm{act}(t)$ in (9) as provided by the measurement unit. We observe that it takes about $0.5\ \mu$s for the measurement circuit to settle to its final value, which determines the time that is required for the matching process.

C. Transmitter-side Matching

We now present results for transmitter-side matching considering the access impedance range discussed in Section V-A. The source impedance of the communication transmitter is set to 50Ω.

This article has been accepted for publication in a future issue of this journal, but has not been fully edited. Content may change prior to final publication. Citation information: DOI 10.1109/TVT.2016.2562629, IEEE Transactions on Vehicular Technology

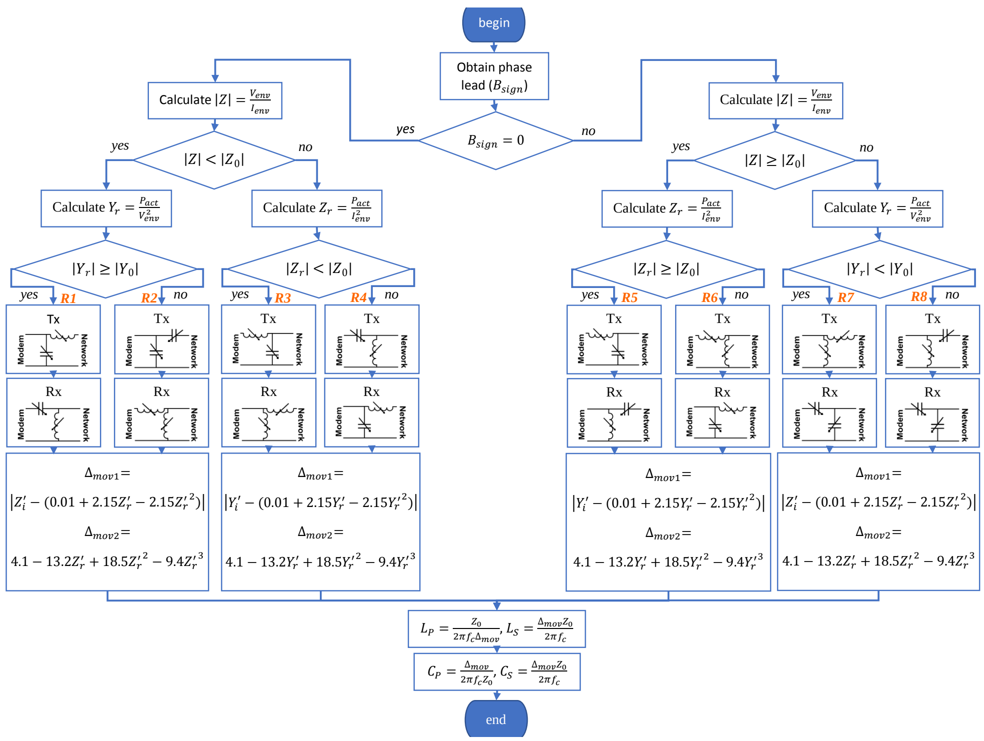

Fig. 12. Flow chart summary of the proposed adaptive impedance matching technique, where "Ri" refers to the region i, identified in Figure 3 and listed in Tables V and VI.

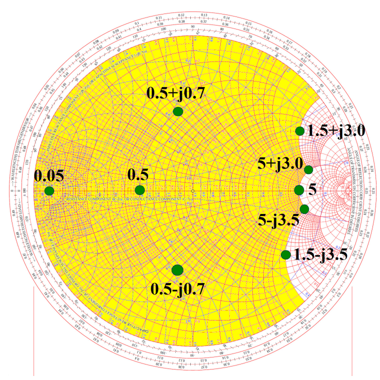

Fig. 13. Coloured area shows the access impedance range for VPLC applications for frequencies between 1-100 MHz [18], [23] and each dot represents a test point. The values on the chart are normalized to 50 Ω.

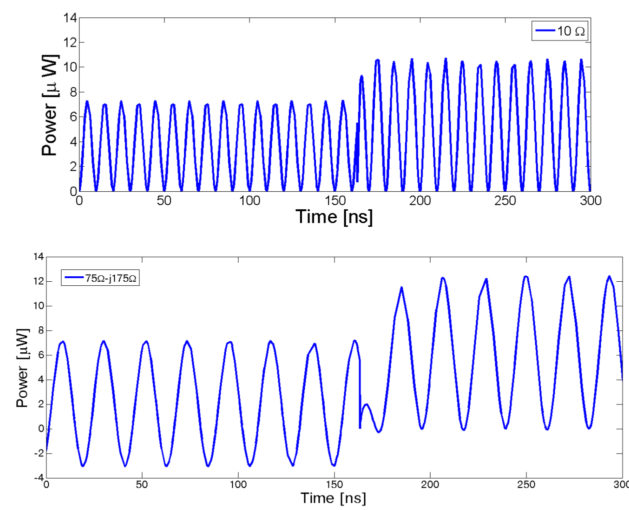

Fig. 14. Illustration of impedance matching considering instantaneous power $P_s(t)$ from the source into the network with an access impedance of 10 Ω (top) and $(75 - j175)$ Ω (bottom), respectively. Impedance matching is activated at $t = 150$ ns.

Figure 16 shows the normalized active power transmitted into the network with and without impedance matching, for different frequencies and access-impedance values. Normalization is with respect to the active power when optimal matching is applied, i.e., a normalized active power of one is the best possible performance. The top and bottom subfigures in Figure 16 are for inductive and purely resistive access impedances, respectively. We observe that for most access-impedance values, impedance matching significantly improves the active power transfer, and that this applies for sampled frequency values from a wide range. The exception is the very low resistance case of 2.5 Ω, for which matching does not show an improvement. We attribute this to rapid changes of the values needed for compensation at the low resistance end, which causes larger estimation errors from fitting susceptance and reactance changes (estimated by (17), (18), (19)). We also note that a wrong estimation in the first move could itself lead to a degraded matching, regardless of the quality of the second move. For all other impedance cases though, matching can improve the power transmission to about 70% and more of the ideally matched case.

Further insight into the performance of our impedance

This article has been accepted for publication in a future issue of this journal, but has not been fully edited. Content may change prior to final publication. Citation information: DOI 10.1109/TVT.2016.2562629, IEEE Transactions on Vehicular Technology

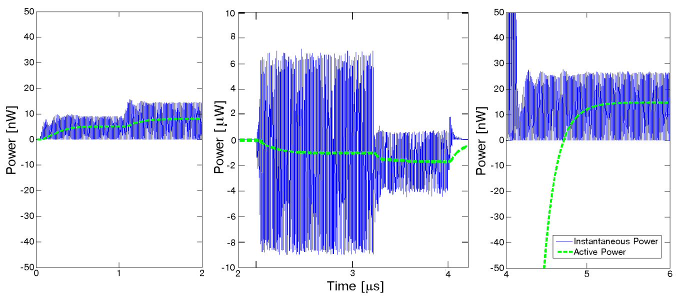

Fig. 15. Illustration of transmitter-side and receiver-side matching for VCU-DC/DC link. Curves are the power received at the receiver of the communication link. Transmitter performs matching at $t = 1$ μs (left subplot). Receiver sends a test signal at $t = 2$ μs to perform matching, which happens at $t = 3.2$ μs (middle subplot). Finally, at $t = 4$ μs, the system goes into data-transmission mode (right subplot).

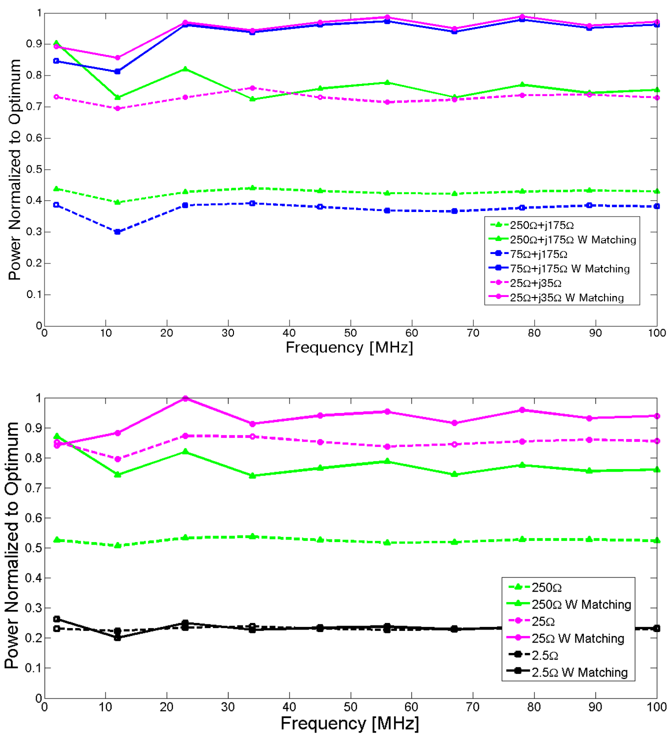

Fig. 16. Normalized active power transferred into the network as a function of frequency with (solid lines) and without (dashed lines) transmitter-side impedance matching for different access impedances. Top: inductive access impedance. Bottom: purely resistive access impedance.

matching solution is provided through Figure 17, which shows the normalized active power transfer as a function of the resistance of a purely resistive access impedance at a frequency of $f_{\mathrm{c}} = 50$ MHz. We observe that impedance matching consistently improves performance, but for the gap to the ideal matching increases drastically for access impedances below about 8 Ω. This could be improved by providing better estimation functions than Eqs. (18) and (19), by, e.g., using a higher-order polynomial expression. We also note that the dimension of the sensing resistor in the measurement unit is critical especially for access impedances with very low resistance. To avoid potential performance degradation because of distorted measurements, the sensing resistor had

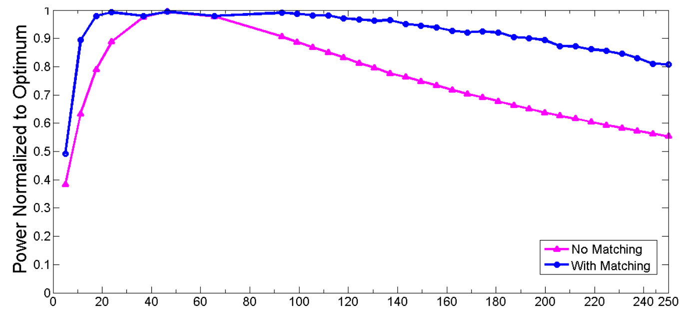

Fig. 17. Normalized active power transferred into the network as a function of resistance for purely resistive access impedance. Frequency $f_{\mathrm{c}} = 50$ MHz.

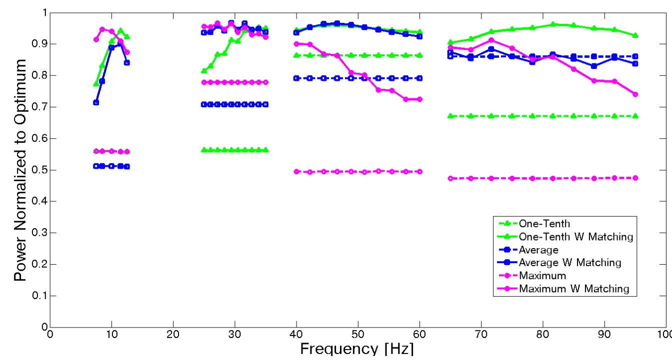

Fig. 18. Normalized active power transferred into the network as a function of frequency with (solid lines) and without (dashed lines) transmitter-side impedance matching. Bandwidth results of the impedance matching for the test cases specified in Table VII.

been chosen as 0.1 Ω.

Finally, in Figure 18 we show the results of the bandwidth simulations according to the parameters specified in Table VII. It can be seen that the matching system shows an overall fairly flat in-band behaviour. Even when there is deviation from the matching frequency f_{c}, still significant improvements of signal-power transfer compared to transmission without matching are achieved. In particular, active power transmitted into the network with matching is always within 30% of the ideal condition. Therefore, under such conditions the matching circuit can be considered as wideband and used for a more broadband signal transmission once fixed and adjusted at a center frequency.

D. *Receiver-side Matching*

The second set of results is for receiver-side matching. The impedance of the communication receiver is assumed to be 50 Ω.

Figure 19 shows the performance, again in terms of normalized power transfer, here from the network into the communication receiver, as a function of frequency and for different capacitive access impedances (top subfigure) and as a function of the resistance of a purely resistive access impedance at $f_{\mathrm{c}} = 50$ MHz (bottom subfigure). We observe that in all cases, the amount of signal power extracted from the network is greatly improved and approaches that of the ideal matching within 30%. A notable similarity to the results from the previous section for transmitter-side matching is the degradation of

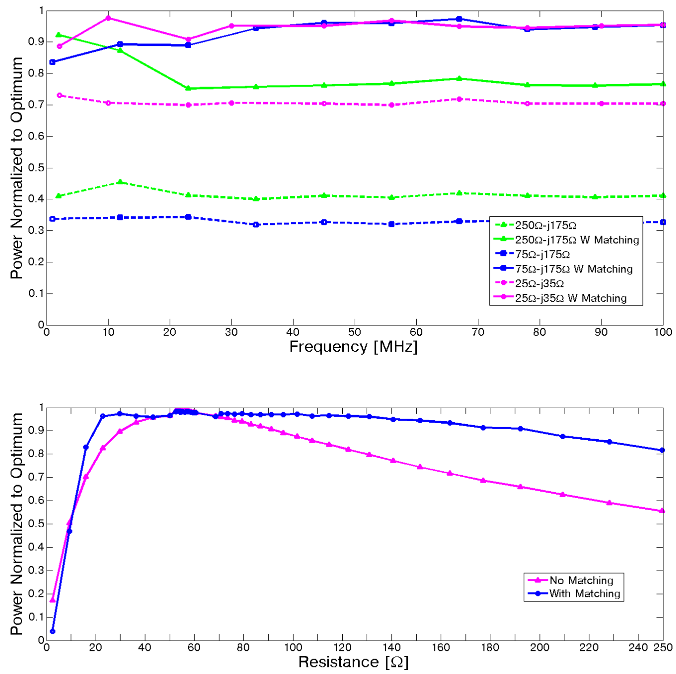

Fig. 19. Normalized active power extracted from the network with and without adaptive impedance matching at the receiver side. Top: Different capacitive access impedance, results with (solid lines) and without (dashed lines) matching as a function of frequency. Bottom: Performance as a function of resistance for a purely resistive access impedance and $f_{\rm c} = 50$ MHz.

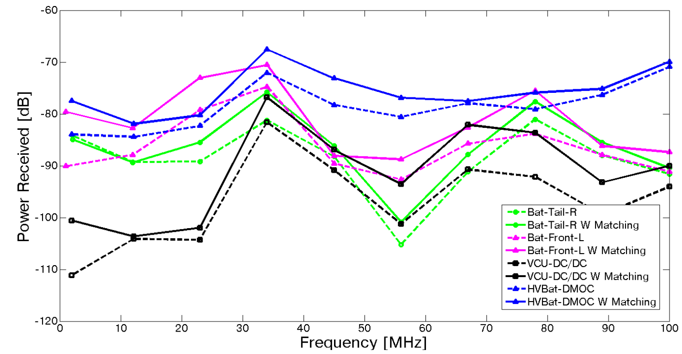

Fig. 20. Active power at the receiver as a function of frequency with (solid lines) and without (dashed lines) impedance matching for four different communication links. In all cases transmitter is a voltage source with an amplitude of 50 mV and both transmitter and receiver have a 50 Ω resistance.

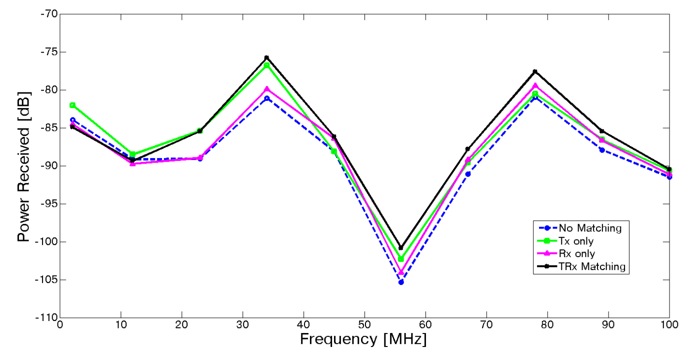

Fig. 21. Active power at the receiver as a function of frequency with (solid lines) and without (dashed lines) impedance matching for the Bat-Tail-R link. Transmitter-side matching (“Tx only”), receiver-side matching (“Rx-only”), and concurrent transmitter- and receiver-side matching (“TRx Matching”) are considered. In all cases transmitter is a voltage source with an amplitude of 50 mV and both transmitter and receiver have 50 Ω resistance.

the transferred power at low-resistance impedances for similar reasons.

E. Matching at Both Ends of the Communication Link

We now show the active power transfer from the transmitter of the communication system to the receiver when the proposed adaptive impedance matching is performed at both ends of the communication link. To evaluate the performance of the system under realistic circumstances of VPLC, the S-parameters obtained in our measurement campaigns [18], [23] were used to describe the network. Figure 20 shows the receiver's active power for transmission with and without matching for four links as a function of frequency. We note that the fluctuation of curves with frequency is due to the frequency-dependent channel attenuation, which affects the measured received power. Comparing the results for with and without matching, we observe improvements in the received power between 1 dB to 10 dB. In other words, up to about 10 times more signal power arrives the receiver due to matching.

To further investigate the distinct effect of matching at each end of the link, Figure 21 shows the received active power for the cases of no matching, only transmitter-side matching, only receiver-side matching, and concurrent transmitter-side and receiver-side matching for one of the links from Figure 20 (the Bat-Tail-R link [23]). We observe that for most frequency values the concurrent matching offers the best performance. The contributions from matching at each end of the link is frequency-dependent though, which is due to the different S-parameters and thus access impedances for different frequencies. Furthermore, in a few instances we note that only transmitter-side matching would result in somewhat higher received power than matching at both ends. In these cases, another adjustment of the matching circuit at the transmitter, after adjustment of the receiver-side matching, would be beneficial.

Finally, the results for bandwidth simulations are shown in Figure 22. Here we selected the Bat-Front-L link from [23] also considered in Figure 20. Matching is done for the frequency points $f_{\rm c} = \{12, 23, 45, 78\}$ MHz and tested in a bandwidth of about $0.2f_{\rm c}$ around the $f_{\rm c}$ value. It can be seen that, in most cases, the matching adjusted at the center frequency of matching leads to an improved power transmission over a wider range around the center frequency. Only for the case of adjusting the matching at $f_{\rm c} = 45$ MHz and operating at above 55 MHz we note a loss in received power due to matching mismatch. We also observe that changes in the power transmission over frequency are often smoother and/or better bounded after matching has been applied. Hence, the proposed matching also improves relatively broadband transmission.

F. Comparison

In order to put the features and results of the suggested design into perspective, we have compared it with the related

This article has been accepted for publication in a future issue of this journal, but has not been fully edited. Content may change prior to final publication. Citation information: DOI 10.1109/TVT.2016.2562629, IEEE Transactions on Vehicular Technology

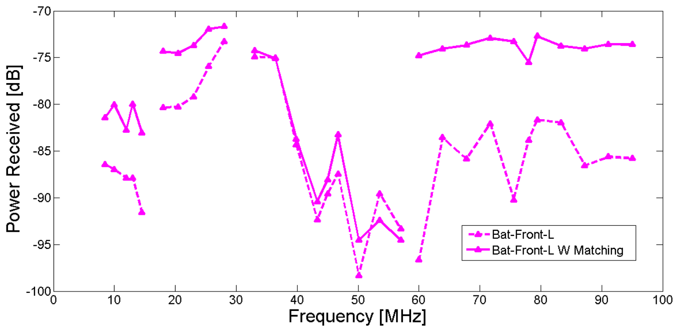

Fig. 22. Active power transferred from transmitter to receiver as a function of frequency with (solid lines) and without (dashed lines) impedance matching for the Bat-Tail-L link. Matching is adjusted at the frequency points $f_c = \{12, 23, 45, 78\}$ MHz. In all cases transmitter is a voltage source with an amplitude of 50 mV and both transmitter and receiver have 50 Ω resistance.

TABLE VIII
COMPARISON OF CURRENT WORK WITH RELATED WORKS.

Work	[29]	[22]	[30]	[31]	This work
Methodology	Analytical	Analytical	Numerical	Analytical	Analytical
Impedance Type	Insertion Loss	Single	Single	Single	Single
Structure	Fixed	Fixed	Flexible	Flexible	Flexible
Implementation	Passive	Combination	Passive	Combination	Combination
Bandwidth	Narrow	Narrow	Wide	Narrow	Narrow/Wide
Frequency (MHz)	13.56	0.132	[1.5-22]	5.5	[1-100]
Impedance (Ω)	[1-100]	[3-10] + j[0.0008-0.83]	[0-400] $\measuredangle$[0-$\pm$75]	[0.32-25.2] + j[5.97-9.3]	[2.5-250] + j[$\pm$4.5-$\pm$175]
Maximum Power Improvement Ratio	N/A	N/A	3.6	7.6	10

work discussion in Section II-B. In Table VIII, we observe that the proposed design achieves the largest maximum power gain (ratio of the power transfer after matching to before matching). Our solution is also tested and proven effective under the widest range of frequencies and loads, with the exception of [30], where a wider range of impedance has been compensated for. However, their maximum achievable power gain is considerably lower than that of the proposed work. Different from [30], which applies a meta-particle swarm optimization algorithm for parameter adjustment, our solution is based on closed-form expressions presented in Section IV, which results in significantly lower computational load. On the other hand, the approach in [30] applies to a wide-band matching, whereas we target narrow-band matching. Our results have shown that the proposed system can be used for a relatively wider band around the design frequency. Being applicable to a wider band around the design frequency is an advantage compared to other narrow-band works listed in Table VIII.

VI. Conclusion

Power line communication (PLC) over the automotive power harness would benefit from impedance matching at the transmitter and the receiver. More specifically, due to the variation of the channel over location and time, adaptive impedance matching is required. In this paper, we presented a design approach for such an adaptive impedance matching system. It includes the actual matching circuitry and a sensing and a control unit to adjust the circuit components. The details of the design were presented, followed by demonstrations of the system performance using simulations for realistic test scenarios. Our numerical results demonstrated that under a wide range of conditions, the proposed design achieves signal-power transfer close to that of optimal matching. Overall power transfer gains achieved due to matching can be up to about 10 dB which is larger than what has been reported in previous works in the literature. Furthermore, whereas our design is for narrow-band transmission, often it also improves the performance for broadband transmission around the nominal matching frequency.

References

[1] N. Taherinejad, R. Rosales, L. Lampe, and S. Mirabbasi, “On the design of impedance matching circuits for vehicular power line communication systems,” in *IEEE International Symposium on Power Line Communications and Its Applications (ISPLC)*, 2012, pp. 322–327.
[2] N. Taherinejad, L. Lampe, and S. Mirabbasi, “Adaptive impedance matching for vehicular power line communication systems,” in *IEEE International Symposium on Power Line Communications and its Applications (ISPLC)*, Mar. 2014, pp. 214–219.
[3] M. Schwartz, “Carrier-wave telephony over power lines: Early history [history of communications],” *IEEE Commun. Mag.*, vol. 47, no. 1, pp. 14 –18, Jan. 2009.
[4] H. Ferreira, L. Lampe, J. Newbury, and T. Swart, *Power Line Communications: Theory and Applications for Narrowband and Broadband Communications over Power Lines*. Wiley, 2010.
[5] S. Galli, A. Scaglione, and K. Dostert, “Broadband is power: internet access through the power line network,” *IEEE Commun. Mag.*, vol. 41, no. 5, pp. 82 – 83, may 2003.
[6] G. Leen and D. Heffernan, “Expanding automotive electronic systems,” *Computer*, vol. 35, no. 1, pp. 88–93, Jan. 2002.
[7] N. Navet, Y. Song, F. Simonot-Lion, and C. Wilwert, “Trends in automotive communication systems,” *Proc. IEEE*, vol. 93, no. 6, pp. 1204 –1223, Jun. 2005.
[8] Strategy Analytics Automotive Electronics report, November 2007, “Automotive Multiplexing Protocols: Cost/Performance Driving New Protocol Adoption,” cited from http://www.businesswire.com/news/home/20071115006121/en/STRATEGY-ANALYTICS-Automotive-Electronics-Network-Market-Stretch, accessed on August 28, 2011.
[9] P. van Rensburg and H. Ferreira, “Automotive power-line communications: favourable topology for future automotive electronic trends,” in *International Symposium on Power Line Communications and Its Applications (ISPLC)*, Kyoto, Japan, Mar. 2003, pp. 103–108.
[10] T. Enders and J. Schirmer, “Automotive powerline communications – a new physical layer for CAN,” in *Int. CAN Conf.*, Munich, Germany, Oct. 2003.
[11] T. Huck, J. Schirmer, T. Hogenmuller, and K. Dostert, “Tutorial about the implementation of a vehicular high speed communication system,” in *International Symposium on Power Line Communications and Its Applications (ISPLC)*, Vancouver, Canada, Apr. 2005, pp. 162 – 166.
[12] W. Gouret, F. Nouvel, and G. El-Zein, “Powerline communication on automotive network,” in *IEEE Vehicular Technology Conference (VTC)*, Apr. 2007, pp. 2545 –2549.
[13] O. Amrani and A. Rubin, “Contention detection and resolution for multiple-access power-line communications,” *IEEE Trans. Veh. Technol.*, vol. 56, no. 6, pp. 3879–3887, 2007.

This article has been accepted for publication in a future issue of this journal, but has not been fully edited. Content may change prior to final publication. Citation information: DOI 10.1109/TVT.2016.2562629, IEEE Transactions on Vehicular Technology

[14] M. Lienard, M. Carrion, V. Degardin, and P. Degauque, "Modeling and analysis of in-vehicle power line communication channels," *IEEE Trans. Veh. Technol.*, vol. 57, no. 2, pp. 670 –679, Mar. 2008.

[15] F. Benzi, T. Facchinetti, T. Nolte, and L. Almeida, "Towards the powerline alternative in automotive applications," in *IEEE International Workshop on Factory Communication Systems*, May 2008, pp. 259 –262.

[16] M. Mohammadi, L. Lampe, M. Lok, S. Mirabbasi, M. Mirvakili, R. Rosales, and P. van Veen, "Measurement study and transmission for in-vehicle power line communication," in *IEEE International Symposium on Power Line Communications and Its Applications (ISPLC)*, Dresden, Germany, Mar.-Apr. 2009, pp. 73 –78.

[17] A. Vallejo-Mora, J. Sánchez-Martínez, F. Cañete, J. Cortés, and L. Díez, "Characterization and evaluation of in-vehicle power line channels," in *Proc. IEEE Global Telecommunications Conference (GLOBECOM)*, Dec. 2010, pp. 1 –5.

[18] N. Taherinejad, R. Rosales, L. Lampe, and S. Mirabbasi, "Channel characterization for power line communication in a hybrid electric vehicle," in *IEEE International Symposium on Power Line Communications and Its Applications (ISPLC)*, 2012, pp. 328–333.

[19] S. Barmada, M. Raugi, M. Tucci, Y. Maryanka, and O. Amrani, "PLC systems for electric vehicles and smart grid applications," in *IEEE International Symposium on Power Line Communications and Its Applications (ISPLC)*, Johannesburg, South Africa, Mar. 2013.

[20] M. Antoniali, M. De Piante, and A. M. Tonello, "PLC noise and channel characterization in a compact electrical car," in *IEEE International Symposium on Power Line Communications and Its Applications (ISPLC)*, Johannesburg, South Africa, Mar. 2013.

[21] V. Degardin, M. Lienard, P. Degauque, E. Simon, and P. Laly, "Impulsive noise characterization of in-vehicle power line," *IEEE Trans. Energy Convers.*, vol. 50, no. 4, pp. 861–868, 2008.

[22] C. Park, K. Jung, and W. Choi, "Coupling circuitary for impedance adaptation in power line communications using VCGIC," in *IEEE International Symposium on Power Line Communications and Its Applications (ISPLC)*, Jeju, Korea, Apr. 2008, pp. 293 –298.

[23] N. Taherinejad, R. Rosales, S. Mirabbasi, and L. Lampe, "A study on access impedance for vehicular power line communications," in *IEEE International Symposium on Power Line Communications and Its Applications (ISPLC)*, Udine, Italy, Apr. 2011, pp. 440 –445.

[24] V. Iyer and S. Makarov, "A lumped circuit for wideband impedance matching of a non-resonant, short dipole or monopole antenna," in *IEEE Antennas and Propagation Society International Symposium (APSURSI)*, Jun. 2009, pp. 1 –4.

[25] D. Pozar, *Microwave engineering*. Wiley-India, 2009.

[26] B. Yarman, M. Şengül, J. Trabert, K. Blau, and M. Hein, "Design of wideband matching networks for wireless communication systems," in *International Symposium on Communications, Control and Signal Processing*, Mar. 2006.

[27] B. Godara and A. Fabre, "Versatile wideband impedance matching circuit based on current conveyors," *Electronics Letters*, vol. 43, no. 6, pp. 37 –38, Mar. 2007.

[28] H. Carlin and J. Komiak, "A new method of broad-band equalization applied to microwave amplifiers," *IEEE Transaction on Microwave Theory Technique*, vol. 27, no. 2, pp. 93–99, 1979.

[29] A. Mavretic, A. Ciszek, and J. Stach, "Apparatus for matching a variable load impedance with an RF power generator impedance," Aug. 5 1997, US Patent 5,654,679.

[30] R. Araneo, S. Celozzi, and G. Lovat, "Design of impedance matching couplers for power line communications," in *IEEE International Symposium on Electromagnetic Compatibility (EMC)*, Aug. 2009, pp. 64 –69.

[31] P. Nisbet, M. He, and L. Zhao, "Transformerless impedance matching networks for automotive power line communication," *Journal of Electrical and Electronics Engineering Research*, vol. 6, no. 2, pp. 13–20, Aug. 2014.

[32] A. Leuciuc and L. Goras, "New general immittance converter jfet voltage-controlled impedances and their applications to controlled biquads synthesis," *IEEE Trans. Circuits Syst. I*, vol. 45, no. 6, pp. 678 –682, Jun. 1998.

[33] Maxim Integrated, "Low-noise amplifier stability concept to practical considerations, part 2. [available online]," http://www.maximintegrated.com/en/app-notes/index.mvp/id/1851, oct 2014.

Nima TaheriNejad (S'08-M'15) received his B.Sc. and M.Sc. degree in electrical and electronic engineering respectively from Nushirvani University of Technology in 2007 and Iran University of Science and Technology in 2009. He received his PhD degree in electrical and computer engineering from the University of British Columbia, Vancouver, Canada, in 2015. He is currently a post-doctorate University Assistant at TU Wien, Vienna, Austria, where his main areas of research are Systems-on-Chip, Self-awareness in Cyber-Physical Systems, Embedded Systems, and Robotics. He has been granted several awards and scholarships from attended universities and conferences. He has authored a book and published in/served as a reviewer for various journals and conferences.

Lutz Lampe (M'02-SM'08) received the Dipl.-Ing. and Dr.-Ing. degrees in electrical engineering from the University of Erlangen, Erlangen, Germany, in 1998 and 2002, respectively. Since 2003, he has been with the Department of Electrical and Computer Engineering, The University of British Columbia, Vancouver, BC, Canada, where he is a Full Professor. His research interests are broadly in theory and application of wireless, optical wireless, power line and underwater acoustic communications. He is currently an Associate Editor of the IEEE WIRELESS COMMUNICATIONS LETTERS and the IEEE COMMUNICATIONS SURVEYS AND TUTORIALS and has served as an Associate Editor and a Guest Editor of several IEEE transactions and journals. He was a (co-)recipient of a number of best paper awards, including awards at the 2006 IEEE International Conference on Ultra-Wideband, the 2010 IEEE International Communications Conference, and the 2011 IEEE International Conference on Power Line Communications. He is a co-editor of the book "Power Line Communications: Principles, Standards and Applications from Multimedia to Smart Grid (2nd ed.) by John Wiley & Sons.

Shahriar Mirabbasi (S'95-M'02) received the B.Sc. degree in electrical engineering from Sharif University of Technology, Tehran, Iran, in 1990, and the M.A.Sc. and Ph.D. degrees in electrical and computer engineering from the University of Toronto, Toronto, ON, Canada, in 1997 and 2002, respectively. Since August 2002, he has been with the Department of Electrical and Computer Engineering, University of British Columbia, Vancouver, BC, Canada where he is currently a Professor. His current research interests include analog, mixed-signal, RF, and mm-wave integrated circuit and system design with particular emphasis on wireless and wireline communications, silicon photonics, RFID, sensor interface, and biomedical applications.